Tellus (1980), *32*, 439–455

Kinematic structure of an Atlantic cloud cluster during GATE and its time variation

By DHIRENDRA N. SIKDAR and STEVEN J. HENTZ[1], *Atmospheric Sciences, University of Wisconsin-Milwaukee, P.O. Box 413, Milwaukee, Wisconsin 53201, U.S.A.*

(Manuscript received November 20, 1979; in final form February 18, 1980)

ABSTRACT

This study uses the GATE (GARP Atlantic Tropical Experiment) upper air network in the tropics combined with high resolution SMS-1 (Synchronous Meteorological Satellite) derived winds at low levels, to identify the time-varying kinematics, and mass flux within the region of an intense cloud cluster on September 5, 1974.

Satellite data was stored, displayed, and processed on the Man-Computer Interactive Data Access System (McIDAS). Measurements of cloud area expansion covering 20 h determined the cloud cluster stages. Quantitative measurements of the mass flux and kinematic properties of the cluster are given for the growth, growth-mature, and mature-dissipating stages of the cluster.

In the growth phase of the cluster strong convergence exists below 900 mb. Relative winds show that the mass inflow to the cluster comes from the west–southwest below 950 mb within the subcloud layer. During the growth-mature stage deep convective system dominates the cluster. Strong low level convergence decreases as divergence at 250 mb becomes dominant. In the growth stage downward motion exists above 600 mb, which becomes strongly upward as the cluster matures. Maximum vertical motion shifts from 800 to 300 mb in the mature-dissipating stage.

A mass budget quantitatively describes the horizontal and vertical mass exchanges in and around the cluster. In the growth stage subcloud layer air is horizontally transported from distances greater than 300 km from the cluster center, transported upward in the cluster, and exits in the 800–600 mb layer. The growth-mature stage, characterized by wide-spread deep convection shows that mass is raised at the 200–250 mb layer, where it is transported northward. Most of this mass is supplied by the large scale flow of warm moist air below 950 mb. Relative winds show that deep convection in the cluster is responsible for the upward transport of equatorial air to higher latitudes, supporting the view that cloud clusters are an integral part of the Hadley circulation cell.

1. Introduction

Recently a number of studies have used GATE data with a view to understanding the relationship between vertical motion and convective activity. Reed et al. (1977) found from their analysis of phase III data that the strongest convergence and upward motion are located somewhat ahead and to the south of 700 mb disturbance center. Nitta (1977) computed budgets of heat and moisture for the A/B scale and found strong upward motion with two maxima, at 700 mb and 350 mb, during active periods of cloud clusters. Frank (1978), from a compositing analysis of 12 convective systems in the B-array, concluded that the vertical motion fields associated with the onset of convection showed a sharp increase in magnitude in the lower levels several hours before the onset of deep convection. In most of these studies area-averaged properties have been used.

In this paper we present a case study of an intense convection on September 5, 1974 during GATE phase III, when a double cloud cluster developed in the A/B ship array (Fig. 1). A number of case studies on this disturbance have since appeared in the journals (Leary, 1979; Leary and Houze, 1979). These studies are mainly based on

[1] Present affiliation: National Weather Service, Forecast Office, NOAA, Louisville, Kentucky 40221, U.S.A.

0040-2826/80/050439-17$02.50/0

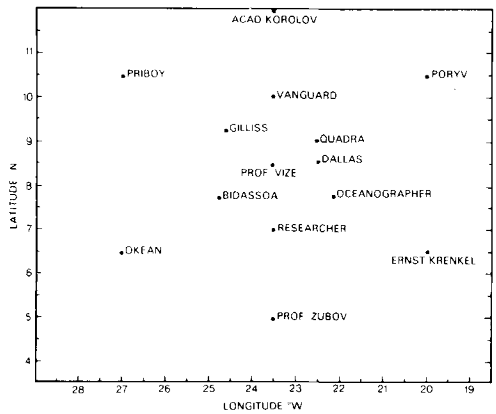

Fig. 1. GATE A/B and B scale ship locations and area covered by grid analysis.

sounding data obtained from the ship array. Suchman et al. (1977) on the other hand, used satellite-derived wind data for September 5, 1974 to study convective mass flux in and around the cloud cluster as a function of time. While these authors demonstrated the feasibility of estimated mass transport from satellite data at two levels using a three-layer model, the role of middle layers remained obscured. The satellite data offers an excellent horizontal resolution in space and time, but in the vertical the resolution is unsatisfactory for very few middle-level cloud tracers could be identified in satellite movie loops, especially in a disturbed situation.

This paper provides another look to the September 5, 1974 disturbance from a compositing of ship soundings and satellite data in a Lagrangian frame. The advantage over other compositing studies (Leary and Thompson, 1976; Smith et al., 1975) is in our ability to see the cluster continuously through its life cycle. The data from ships are time-composited with respect to the western cloud cluster location (Fig. 2) determined on the McIDAS (Smith, 1975). Time compositing radiosonde data enables the upper tropospheric flow to be determined, and with the addition of satellite derived low level winds created an excellent data set for the study of the convective mass transport in the region of a cluster.

2. Data sources

2.1. *Conventional data*

Radiosonde data for this study were obtained from the Center for Experimental Design and Data Analysis, NOAA. Russian ship data include the dynamic and thermodynamic parameters of pressure, height, temperature, relative humidity, wind speed and direction, for the standard and significant levels. U.S. and Canadian ship data include 5 mb resolution parameters of pressure, height, temperature, specific humidity, and u, v components of the wind. The U.S. and Canadian data were generated from its raw form by a series of processing steps (U.S. Gate Office, 1977). Approximately 140 radiosonde soundings from 0000 GMT on September 5, 1974 to 0000 GMT

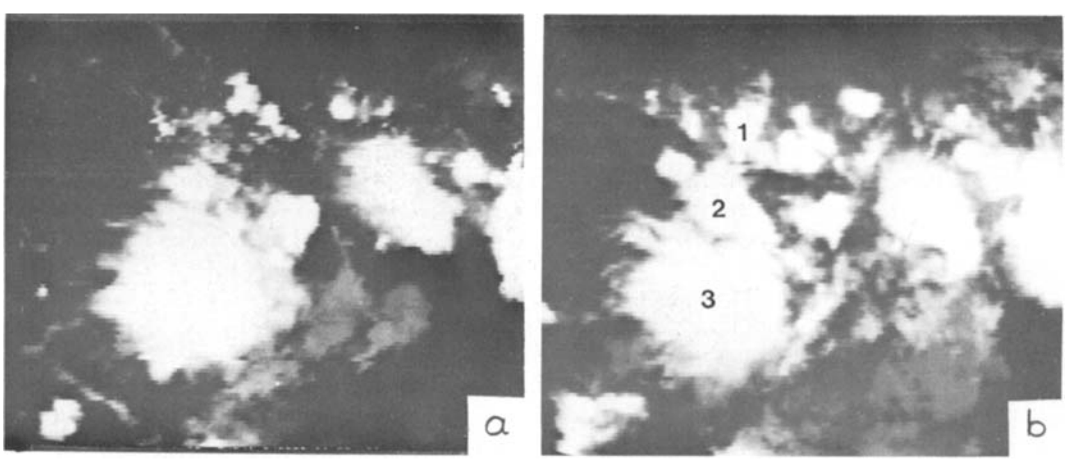

Fig. 2. SMS-1 7.4 km resolution at (a) 0400 GMT and (b) 0600 GMT on September 5, 1974.

on September 6 make up the conventional upper air data set.

Overall the quality of the GATE data is good. However, problems do exist in comparing U.S. and Russian wind observations due to differences in their tracking systems (Reeves, 1978). To solve these problems the composited winds were plotted and wind vectors inconsistent with the general flow pattern were deleted. The remaining winds were placed into an objective wind analysis program (Mancuso and Endlich, 1973) which uses a least square fitting of the initial wind observations.

2.2. *Satellite data*

During the summer of 1974, the synchronous meteorological satellite (SMS-1) was positioned over the GATE area. Images every 30 min were obtained with a maximum resolution of 0.92 km for visible, and 7.4 km for infrared images. While visible images were only available during daylight hours, infrared data were available 24 h a day. A 24-h sequence of infrared and visible images on September 5 were stored and displayed on our McIDAS terminal. The software of McIDAS allowed the mapping of cloud height, base, and thickness using cloud top temperature (Mosher, 1975).

3. Data analysis techniques

Upper air data were taken on ships positioned in two hexagons (Fig. 1). The inner array of ships in an approximate hexagonal pattern is called the B array, while the outer hexagon is called the A/B array. Ships spread outside the A/B array form the A or synoptic scale.

In the time compositing technique used in this study, the motion of the cloud cluster must be accurately determined. This was accomplished by observing a 24-h sequence of enhanced visible and infrared SMS-1 images. Movement of bright cores on the enhanced images, assumed to be areas of deep convection (Martin and Suomi, 1972), were tracked and averaged on the McIDAS system. Following the movement of the center of deep convection gives a more accurate representation of the cluster's motion, since the influence of spreading cirrus is eliminated.

Radiosonde data from the A/B, B and 2 A scale ships were composited for 3 periods (0000 to 1200 GMT, 0600 to 1800 GMT, and 1200 to 2400 GMT on September 5) at 15 levels from 1000 to 100 mb. In determining the time variation of the kinematics of the cluster, the 12-h composites with nominal times 0600, 1230, and 1800 GMT were used. The 1230 GMT nominal time was chosen to correspond to the satellite-derived wind sets of Suchman and Martin (1976).

Low and high level winds for 0900, 1230, and 1500 GMT have been computed on McIDAS by tracking small cumulus and cirrus cloud tracers by Suchman and Martin (1976). They show that the satellite-derived low and upper level winds correspond to 950 and 250 mb winds. Therefore, to better represent the low level flow the high density satellite-derived winds are added to the composited 950 mb radiosonde winds. High level satellite-derived winds were not used in the composites because of the difficulty in assigning a single height level to the cirrus tracers. In addition, the upper level wind flow is rapidly changing and the addition of the 0900 and 1500 GMT high level satellite-derived winds in the 0600 and 1800 GMT nominal composites would bias the results toward the active period of the cluster (0900 to 1500 GMT).

In the actual calculations radiosonde data are placed into a grid point analysis program (WIND*SRI) developed at the Stanford Research Institute (Mancuso and Endlich, 1973). This program has been used to obtain composited wind fields by specifying the nominal time, length of time composite, and cloud cluster velocity. Wind observations are displaced along a line parallel to the motion vector of the cloud cluster. The amount of displacement of a wind observation is proportional to its deviation from the nominal time. Grid points every 0.5 degree are obtained for an area 8° latitude by 10° longitude centered on the B scale array. Grid point values of u and v components are calculated by a least square fitting of a first degree polynomial to a present number of wind observations within a specified search radius. For this study the closest 8 winds 333 km are used. In the grid point calculations the observations are weighted inversely with distance. Divergence and vorticity fields are calculated by finite differences of the grid point u and v values. For computing the vertical profiles of u and v components, grid point values are averaged inside a circle of radius 1.5° centered on the deep convection, determined by enhanced satellite images.

As stated earlier the low level satellite-derived winds correspond to the 950 mb level. Convergence in the cluster calculated from the composited ship winds at 950 mb is found to be less than the convergence obtained from the data set including both the composited 950 mb ship winds and low-level satellite-derived winds, suggesting that the ship composites under-estimate the actual convergence. The lower magnitude is probably a result of poor spatial resolution of the composited ship winds in the region of a wind shift line between southwest and northeast winds in the vicinity of the cluster. Convergence obtained by low level satellite data alone is not sufficient since cirrus outflow shields the low level cumulus tracers. The convergence obtained by including both ship and satellite-derived winds is considered more representative of the actual convergence.

Convergence calculated from the 950 mb ship and satellite-derived winds is assumed valid for the 1000 mb level, since the ship composites at both of these levels show almost the same convergence value. The actual composited ship winds are used for all other levels. A further verification for the use of the satellite winds is the fact that the vertical mass balances much more closely with the addition of the satellite-derived winds.

Vertical motion is computed for 15 levels in the atmosphere, by applying equation of continuity to the averaged grid point divergence values. Integrating the equation of continuity,

$$\left(\frac{\partial \bar{u}}{\partial x} + \frac{\partial \bar{v}}{\partial y}\right)_p + \frac{\partial \omega}{\partial p} = 0 \qquad (1)$$

gives the vertical motion at the top of each level between 1000 and 100 mb (with the boundary conditions of zero vertical motion at the surface and at 100 mb) by,

$$\omega_p = \omega_{p+\Delta p} + \left(\frac{\partial \bar{u}}{\partial x} + \frac{\partial \bar{v}}{\partial y}\right)_p \Delta p$$

where

$\bar{u}$ = average u component
$\bar{v}$ = average v component
p = a constant pressure surface
ω = vertical velocity in mb s^{-1}
Δp = depth in mb between two pressure levels

The divergence and vertical motion profiles are adjusted according to a technique developed by O'Brien (1970). This technique gives a smaller weight to the upper level divergence and vertical motion. The adjusted divergence D' and vertical motion ω' are given by

$$D_k' = D_k + \frac{k}{M}(\omega_K - \omega_T)/\Delta p \qquad (3)$$

and

$$\omega_p' = \omega_p - (\omega_K - \omega_T)\frac{k}{2M}(K + 1) \qquad (4)$$

where

$$\bar{D}_k = \left(\frac{\partial \bar{u}}{\partial x} + \frac{\partial \bar{v}}{\partial y}\right)_p, \text{ and } M = \sum_{k=1}^{K} k = \tfrac{1}{2}K(K+1)$$

In these equations K is the total number of layers, while k denotes the individual layers. For the vertical motion equation ω_K' is the unadjusted vertical motion at the top layer (100 mb), and ω_T is the specified boundary condition of the vertical motion at the top layer (100 mb). In this study, we assume $\omega_T = 0$ at 100 mb, the approximate tropopause height.

4. Results

4.1. *The convective disturbance*

September 5, 1974 was one of the most convectively active days over the GATE A/B array. The cluster developed along a wind shift line at approximately 0400 GMT, seen as a band of clouds, extending northwest to southeast across the Vanguard (Fig. 2). The cluster showed a nearly steady southwestward motion (55°, 8.2 m s^{-1}), from 0400 to 1600 GMT.

Observations from the Vanguard (Fig. 3) show winds shifting from west-northwest to north as the cloud band passes at 0330 to 0405 GMT at the Vanguard. Satellite-derived cloud tops indicate only a few cumulonimbi reach 250 mb.

Convection continues to grow along the line as it moves sothwestward. At 0530 GMT individual areas of deep convection begin to merge forming the band #1 of 3 convective bands seen in the 0600 GMT infrared image (Fig. 2b). Band #2 is a relatively stationary area of thundershower activity. Band #3 is the dissipating remnants of a

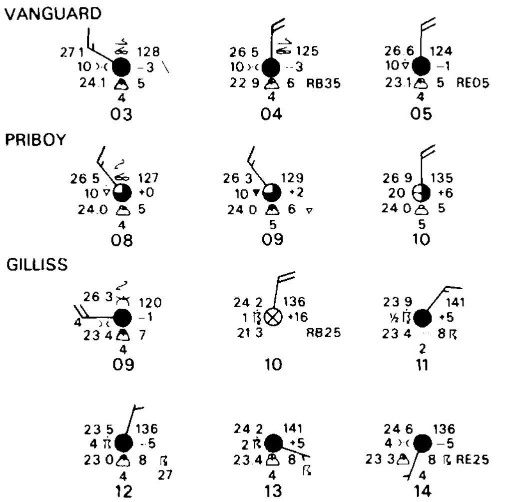

Fig. 3. Selected surface ship observations from Vanguard, Priboy, and Gilliss. Temperatures are in °C and visibilities in km. One barb is 5 m/s. Three-hourly precipitation is in millimeters.

once active cloud cluster. Band #1 gradually overtakes band #2 at 1100 GMT. The merged cloud system continues to move southwest at 8.2 m s^{-1}. The cluster to the east will not be discussed here.

As evident in the satellite images (Figs. 2, 4 and 5) convection inside the cloud cluster is much more intense after 0830 GMT than when the system passed the Vanguard at 0330 GMT. Moderate to heavy thunderstorms occur at the Gilliss from 1000 to approximately 1130 GMT. Visibilities are restricted to only 0.5 to 1.0 km during heavy rainfall. As the heaviest thunderstorms pass, winds shift to the north.

New convection develops at the northwest end of the cloud cluster, along with the cloud band that extends to the northwest (Fig. 4). Earlier at 0930 GMT this cloud band passed the Priboy. Surface observations indicate that the cloud band consists of towering cumuli and cumulonimbus clouds with light to moderate showers. As the cloud band passed the Priboy winds shift from northwest to north and increase in speed from 6.0 to 9.0 m s^{-1}.

A rapidly expanding cirrus canopy begins to spread from the cluster at 1230 GMT (Fig. 4b). Satellite images show the massive cirrus surrounding the western cluster at 1800 GMT (Fig. 5a). After 1600 GMT the cluster showed a more westerly movement. This more westerly track is the result of convection developing on the northwestern edge. The cirrus surrounding the cluster begins to dissipate at 2100 GMT (Fig. 5b).

The cirrus area and expansion rate is a good measure of intensity of convective activity (Sikdar and Suomi, 1971, 1972). With the use of McIDAS the area of the cloud cluster and its cirrus shield is measured on a series of infrared images. A software program calculates the cloud area greater than up to 8 preset satellite digital values. These digital values (D.V.) are converted into equivalent blackbody temperatures. The equivalent blackbody temperature is approximately the cloud top temperature when clouds are thick (Mosher, 1976). These temperatures were compared to the Gilliss soundings and assigned a pressure value.

The area of cloud tops higher than 200, 175, and 150 mb (Fig. 6) gives the best indication of the cloud cluster's life cycle by showing cloud tops of active deep convection. The period 0000 to 1200 GMT is the growth-mature stage. During this time the area of cloud tops above 200 and 175 mb increased and peaked between 1400 and 1430 GMT. The area of cloud tops higher than 150 mb peaked earlier at 1300 GMT. The coldest satellite-derived cloud tops were measured to be 198 K (105 mb), the tropopause height. Assuming the active portions of thunderstorms are shown by cloud tops penetrating the cirrus shield at 200 mb, thunderstorms occupy at most 20% of the cluster area during the mature stage. From 1300 to 2400 GMT cloud area decreased, first at the highest levels, then at lower levels. This period is the mature-dissipating stage of the cluster. Cloud tops decay rapidly above 175 mb after 2100 GMT, while tops above 350 mb decrease only slowly indicating cirrus and middle level cloudiness, remain for a much longer time. The cirrus shield (cloud tops higher than 350 mb) ceases to expand 3.5 h after the cluster is seen to be most active. The cirrus shield expands at an almost constant rate until it decreases.

The twelve-hour composites are used to study the various stages in the satellite observed cluster lifetime. The 0600 GMT nominal composite describes the growth stage; the 1230 GMT nominal composite describes the growth-mature stage; the 1800 GMT nominal composite describes the mature-dissipating stage, These stages are not intended to describe distinct phases in the lifetime of the cluster, but rather describe what is observed in the satellite images over the given 12 h period.

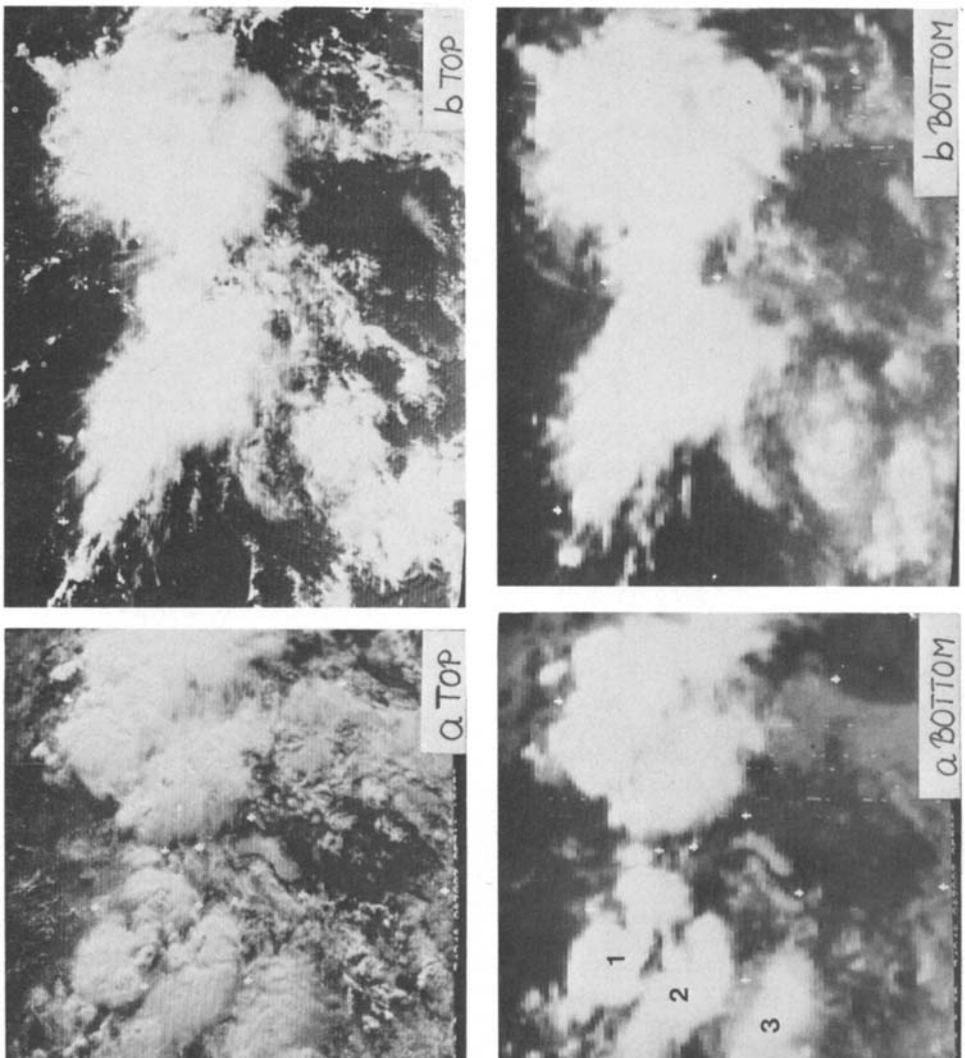

Fig. 4. SMS-1, 1.8 km resolution visible and 7.4 km resolution infrared images on September 5, 1974 at (a) 0830 GMT and (b) 1230 GMT. The cluster to the west is under study. GATE A/B and B scale ships are marked by (+).

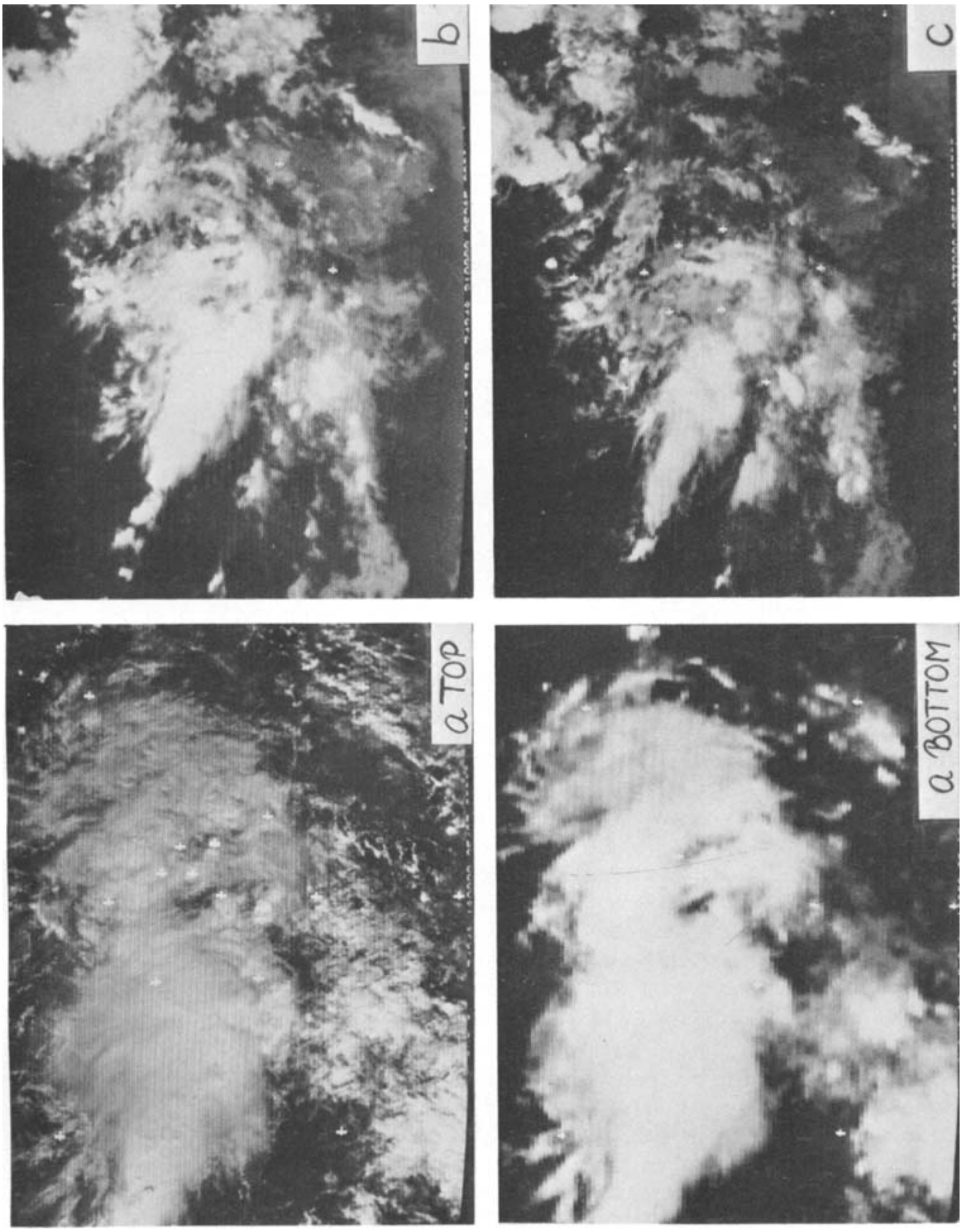

Fig. 5. SMS-1 1.8 km resolution visible and 7.4 km resolution infrared images on September 5, 1974 at (a) 1800 GMT; (b) SMS-1 7.4 km resolution infrared image at 2100 GMT; (c) SMS-1 7.4 km resolution infrared image at 2330 GMT.

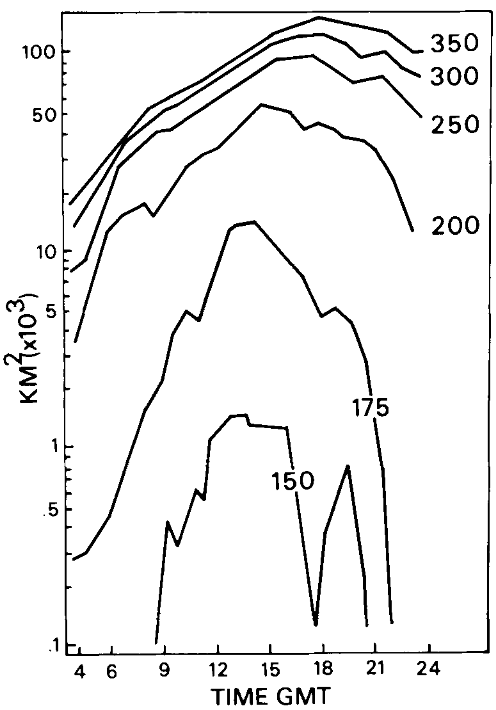

Fig. 6. Cloud cluster area expansion for cloud tops higher than 350, 300, 250, 200, 175, and 150 mb.

4.2. *Wind fields*

Winds relative to the cloud cluster (Fig. 7) were obtained by subtracting the motion of the cluster from the wind fields. The 950 mb relative wind field shows that almost all of the inflow into the cluster is from the southwest, the leading edge of the cluster. The 200 mb wind field shows that the outflow from the cluster is entirely to the north. Winds relative to the cluster are quite similar to those found by Houze (1977) in studying a different GATE, tropical squall line on September 4–5.

4.3. *Vertical wind profiles*

Fig. 8 shows the zonal and meridional wind components for the cloud cluster area from this study and the GATE mean obtained from Gray et al., U.S. Gate Office (1977). Although the flow in the cluster area is similar to the GATE mean, several departures are seen. The zonal wind profile in the cluster shows that below 800 mb, the westerlies are stronger than the GATE mean. There is little difference in the middle levels, while in the upper tropospheric divergence layer the easterlies are weaker than the GATE mean. The level of the maximum upper tropospheric easterly flow is about 50 mb higher than the mean profiles. Strongest vertical shear is seen at the 600 and 150 mb wind maxima. Fig. 8 clearly shows that the easterlies decrease with time from 800 to 300 mb, quite possibly the result of general upward motion, transporting low level westerly momentum.

As evident in the satellite images the cluster exhibits many features of a squall line. A NW–SE line of cumulonimbi moving at a fairly rapid speed 8.2 m s^{-1} (Fig. 8a) resembling Frank's (1978) mean zonal wind profile of 4 composited squall lines that show strong surface to 650 mb and 650 to 200 mb vertical wind shear. In the meridional profile (Fig. 8b), a pronounced increase of the northerly flow indicates that the cluster is located west of an approaching easterly wave. In Riehl's classic Caribbean case (1954), the wave moved slower than the current and the disturbed weather was found to the east of the axis. In this case study we interpret the wave to be moving faster than the current for the disturbed weather to be located to the west of the axis. In the layer 500 to 350 mb, meridional flow is from the south, in response to a trough, whose axis runs southwest across the cluster. The small southerly values at 250 and 200 mb are caused by the diffluence line across the cluster. A similar condition arises at the low level convergence line. Vertical shear is relatively constant with height. The observed meridional wind structure is again similar to Frank's (1978) squall line profile except northerly flow below 700 mb is much stronger in the September 5 case. Very little change in the meridional flow is indicated over the lifetime of the cluster.

4.4. *Zonal and meridional cross-sections of wind*

North–south cross sections of the zonal and meridional wind fields across the cluster were obtained from plotting grid point u and v components.

The N–S zonal wind cross section (Fig. 9) shows the same pattern as the composited Reed et al. (1977) zonal mean wind field from phase III of GATE. The westerly monsoon wind maximum occurs at 950 mb south of the cluster. Near the cluster westerlies are confined below 800 mb. A middle tropospheric easterly wind maximum of 15 m s^{-1} exists at 150 mb, 400 km south of the cluster.

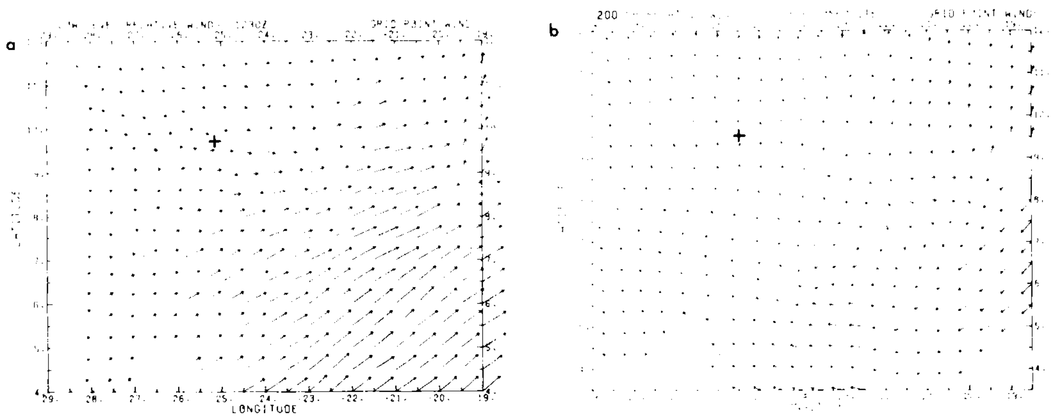

Fig. 7. 1230 GMT composited relative wind field for (a) 950 mb and (b) 200 mb. 1230 GMT cloud cluster mass weighted center is indicated by (+).

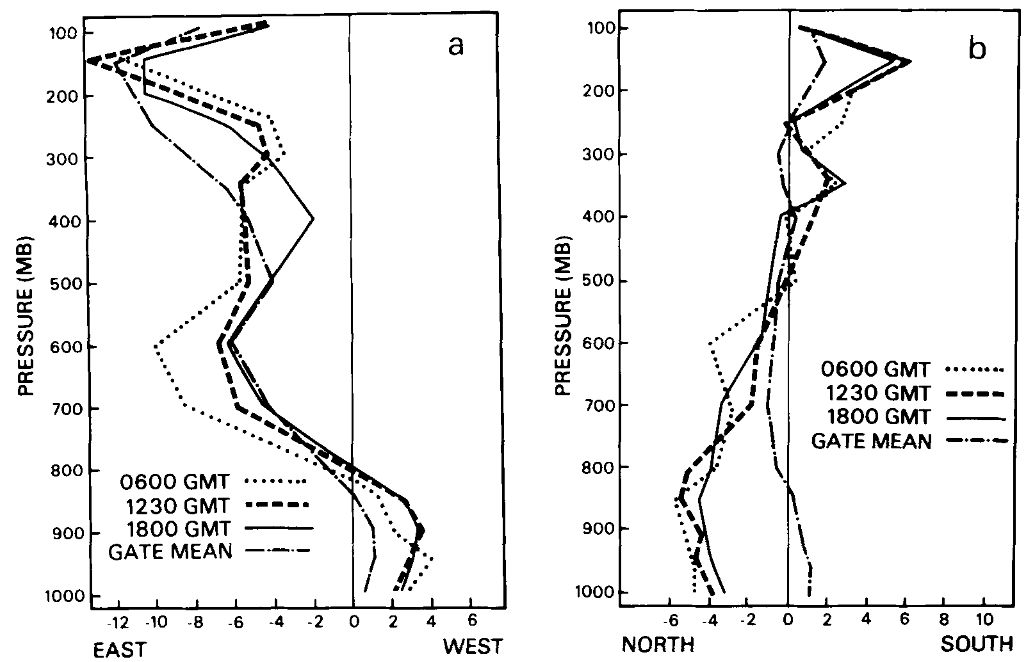

Fig. 8. Vertical profiles of average (a) zonal and (b) meridional wind components (m/s) for the cluster and the GATE mean obtained by Gray et al. (1977).

Vertical and horizontal shears are large in the vicinity of these wind maxima, with the cluster located in the cyclonic shear zone of the middle level easterly wind maximum.

Fig. 10 shows the N–S cross section of the meridional flow of the 1230 GMT composite. Northerly flow dominates the middle and lower troposphere. Below 900 mb southerly flow is seen

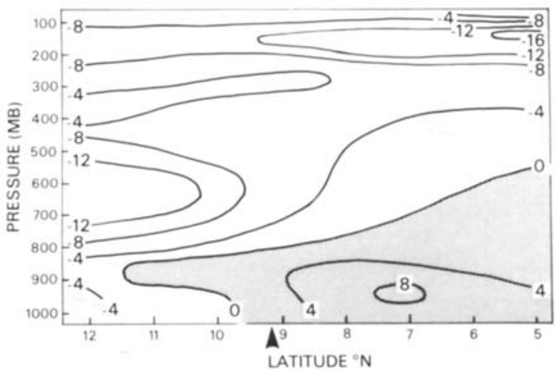

Fig. 9. Zonal wind (m/s) along 25.5°W for 1230 GMT composite. The cloud cluster center is marked by (↑).

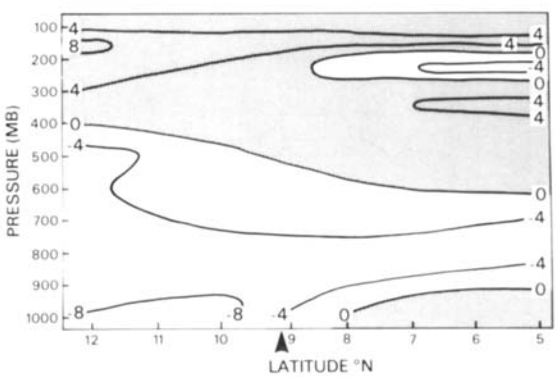

Fig. 10. Same as Fig. 9, except for meridional wind (m/s) at 1230 GMT.

south of the cluster center. The 200 and 250 mb diffluence axis is clearly seen over the cluster by a narrow region of northerly flow at 250 mb.

4.5. *Kinematic profiles*

The cloud cluster-scale divergence profiles for the 0600, 1230, and 1800 GMT composites are given in Fig. 11. In the growth phase of the cluster (0600 GMT composite) strong convergence occurs in the lower level (up to 900 mb). The middle levels are divergent from 850 to 500 mb. Two divergence maxima are seen. Maximum divergence (2.2×10^{-5} s^{-1}) at 600 mb is due to the middle level easterly wind maximum with strongest gradient to the north-west of the cluster. Convergence dominates in the upper levels, except at 250 mb where a second weaker divergence maximum (1.2×10^{-5} s^{-1}) is located. Strong low level convergence with strong middle tropospheric divergence is favorable for the increased development of larger cumulus clouds.

The 1230 GMT composite represents a period when deep convection increases and reaches a maximum. During this period the depth and magnitude of the low level convergence increase. The middle level divergence maximum disappears and becomes almost non-divergent from 800 to 400 mb as the cluster develops. At the same time the 250 mb divergence maximum becomes dominant at upper levels.

By 1800 GMT a large dense cirrus shield spread from the deep convection. Infrared satellite images showed that after 1800 GMT cumulus convection still remained active in the cluster, but occupied a smaller area. The upper level divergent outflow maximum becomes the dominant feature with maximum divergence (4.8×10^{-5} s^{-1}) at 200 mb. Low level convergence decreased and becomes slightly divergent at 800 mb, possibly due to large-scale sinking motion or small scale cool convective downdraft (Zipser, 1977). From 700 to 325 mb weak convergence replaces the divergent

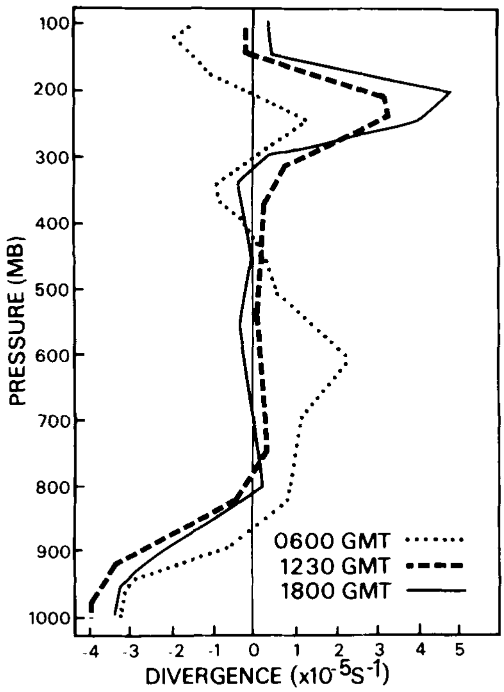

Fig. 11. Vertical profiles of average divergence ($\times 10^{-5}$ s^{-1}) for the cloud cluster for the 0600, 1230 and 1800 GMT composites.

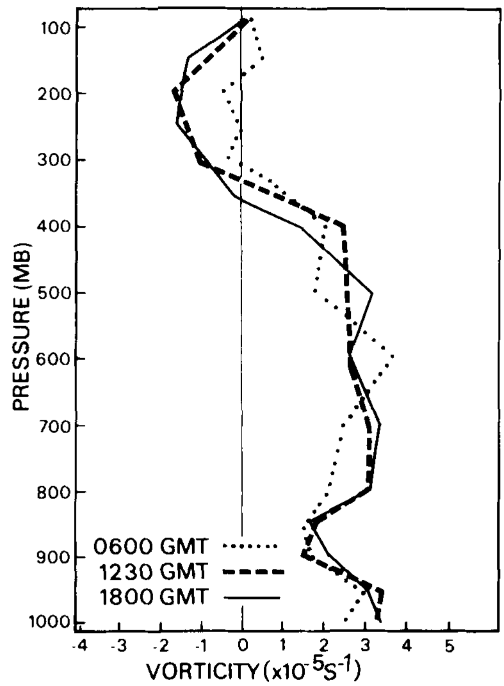

Fig. 12. Vertical profiles of average vorticity ($\times 10^{-5}$ s^{-1}) for the cloud cluster for the 0600, 1230 and 1800 GMT composites.

layer. This transition along with the information of divergence around 800 mb is similar to what Nitta (1977) found in dissipating GATE cloud clusters.

4.6. *Vorticity profiles*

The vorticity profile is shown in Fig. 12. Overall the vorticity field for the cloud cluster does not change much over time. Below 900 mb, little vorticity change with time was observed despite the strong convergence. A strong positive vorticity is present at lower levels even in the incipient stages of the cluster.

The decrease in positive vorticity at 900 and 850 mb is seen as the transition between the subcloud inflow layer and the middle layer flow. Below this transition zone positive vorticity is mainly due to cyclonic shear between the monsoons and trades. Near the cluster at 900 and 850 mb the flow is northerly with little horizontal shear or curvature. From 700 to 600 mb positive vorticity is the result of the cloud cluster being located in the cyclonic shear zone of the easterly wind maximum. The large positive vorticity at 500 and 400 mb is due largely to cyclonic curvature of the trough just east of the cluster. The developing cluster has little effect on the vorticity below 350 mb, perhaps due to the fact that large-scale features are the primary cause of the observed vorticity profiles. The increase in upper tropospheric divergence with resulting negative vorticity is clearly the response to the deep convection in the cloud cluster.

4.7. *Vertical motion*

Vertical motion for the three composites are seen in Fig. 13. The 0600 GMT composite shows upward vertical motion below 600 mb. Downward motion from 600 to 100 mb may be due to sinking motion from the very active eastern cloud cluster during the early growth phases of the western cluster under study here. This downward motion becomes very strongly upward in the 1230 GMT composite. As a result cumulonimbi in the cluster multiplied and intensified, as seen in the satellite images (Figs. 2, 4 and 5). Maximum vertical motion shifts from 800 to 300 mb from the 1230 to

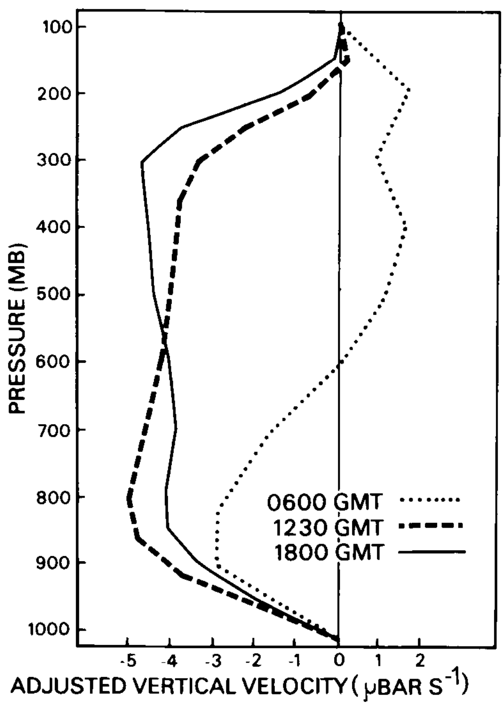

Fig. 13. Vertical profiles of vertical motion (μbar s^{-1}) for the cluster for the 0600, 1230 and 1800 GMT composites.

1800 GMT composite, due to the predominance of deep convective clouds.

Vertical motion across the motion vector of the cloud cluster is computed from the divergence cross section and adjusted using eqs. (3) and (4). At the 0600 GMT nominal time (Fig. 14a), the cluster develops in a broad region of upward motion extending to 600 mb. Maximum vertical motion of 4.5 μbar s^{-1} is at 850 mb. Near the center of the cluster, a narrow region of upward motion extends to 300 mb. In the middle and upper levels of the cluster environment general downward motion is observed.

As the convection inside the cluster grows and reaches its maximum state the upward motion field increases to 150 mb, extending in the horizontal across 300 km (Fig. 14). Strong vertical motions of $-5.0\,\mu$bar s^{-1} are found at the center of the cluster. Maximum vertical motion increases to -7.4 μbar s^{-1} at 800 mb in the 1230 GMT nominal composite. Sinking motion is seen both ahead and behind the cluster. Satellite images (Fig. 4) shows a lack of low and middle level cloudiness in both these regions. Winds relative to the cluster indicate inflow into the leading edge with outflow behind the cluster. Therefore, the compensating sinking motion for the cluster is predominantly at the trailing edge (north to northeast).

Maximum vertical motion is shifted upward and located at 400 mb in the mature-dissipating stage (1800 GMT composite). A tilt of the upward motion with height toward the rear of the cluster is indicated in the cross sections (Fig. 14). This tilting is located downward of the relative flow. Downward motion 250 km southwest and 240 km northeast of the cluster intensifies with maxima at 500 mb (Fig. 14c).

4.8. *Mass budget*

A budget box of the vertical and net horizontal mass flux for the cluster is portrayed in Figs. 15, 16 and 17. Flux values start with a 1° cylinder centered at the cloud cluster center. Fluxes for additional rings around the 1° cylinder are given every 0.5° latitude.

Vertical mass flux is expressed by

$$\bar{M} = \bar{w}\bar{\rho}\bar{A}$$

$\bar{M}$ is the average vertical mass flux for a given area $\bar{A}$, with mean density $\bar{\rho}$ and mean vertical motion $\bar{w}$ at 15 levels for given circles with area $\bar{A}$ encompassing the cluster. Vertical motion $\bar{w}$ is computed by averaging grid point divergence values for each level inside the circle, applying the equation of continuity, and adjusting the results by eqs. (3) and (4). Horizontal mass flux is computed for a particular layer by subtracting the vertical mass flux at each layer's bottom surface from the top surface.

In computing the budget box the vertical mass flux for the cylinder of 1° is plotted for 15 levels. Vertical mass flux for the 1.25° ring is obtained by subtracting the vertical mass flux of the 1° circle from the 1.5° degree circle. Net horizontal mass transport for the 1° circle is obtained by subtracting adjacent vertical flux values. The same procedure is followed for each additional ring.

Figs. 15, 16 and 17 show the interaction of different scales of motion. In the evolutionary-growth stage of the cluster a large amount of mass is transported below 800 mb, from outside the 2.75° ring, towards the center of the cluster (Fig. 15). The center 1° cylinder and each successive

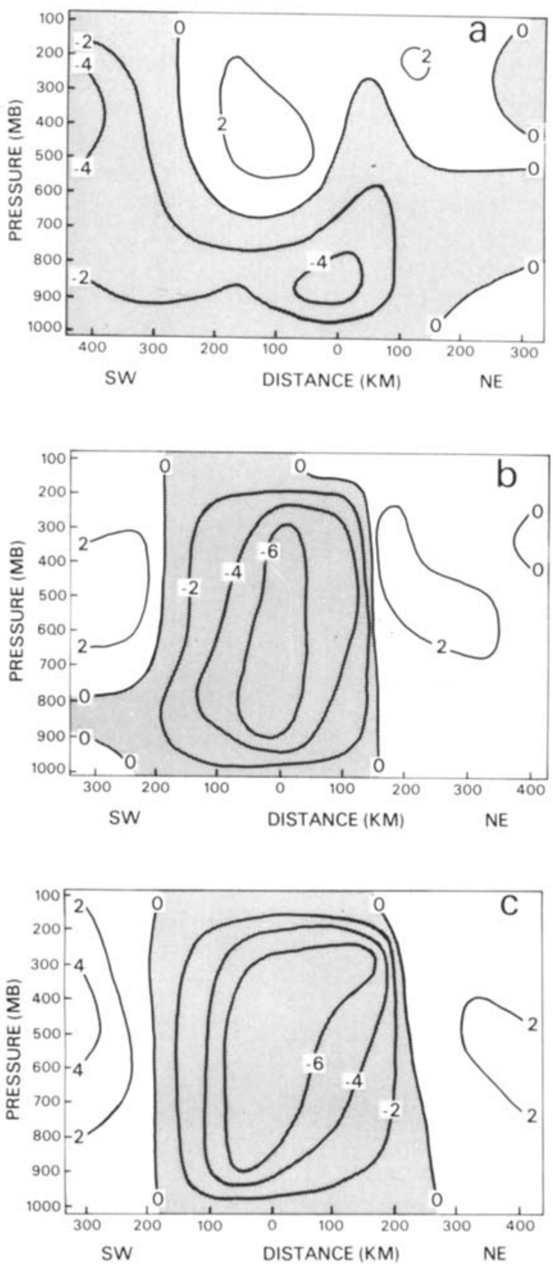

Fig. 14. Cross sections of vertical motion (μbar s^{-1}) across the direction of motion of the cloud cluster for the (a) 0600 GMT, (b) 1230 GMT, (c) 1800 GMT composites. "Zero" km corresponds to the cloud cluster center.

ring shows almost the same vertical mass flux (12 $\times$ 10^8 kg s^{-1}) at 800 mb. This implies a broad area of mass convergence in and around the cloud cluster. The large vertical mass fluxes for the 2.75° ring are the result of a previous cloud cluster that was active around 0100 GMT. All of the mass transported below 900 mb into the 1° cylinder and 1.25° ring is transported back to the outer rings in the 800 to 600 mb layer. Vertical motion is almost zero at 600 mb. It is obvious that deep convection is not widespread with 1.5° radius in the 0600 GMT mass flux computations. A second cir-

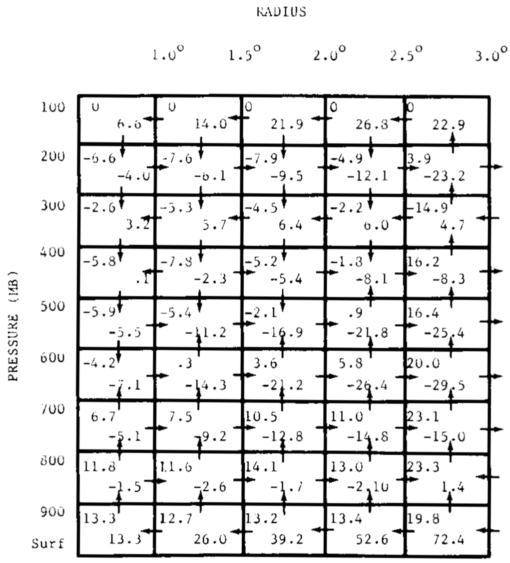

Fig. 15. Budget box of the vertical and net horizontal mass flux (10^8 kg/s) for the 0600 GMT composite, centered about the cluster. Horizontal flux values are in the lower right hand corner and vertical flux values are in the upper left hand corner.

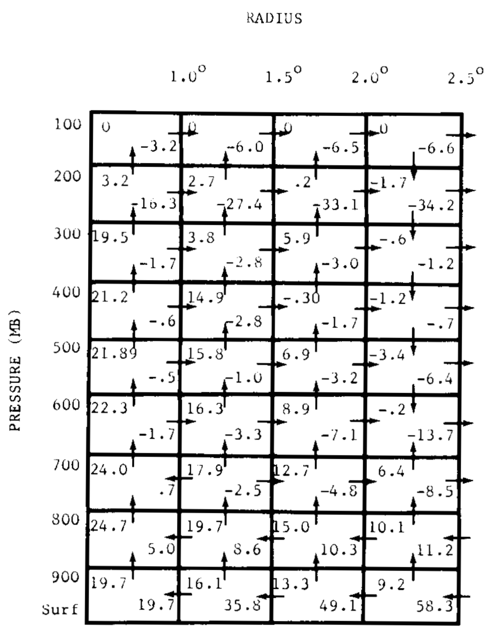

Fig. 16. Same as Fig. 15, except for 1230 GMT.

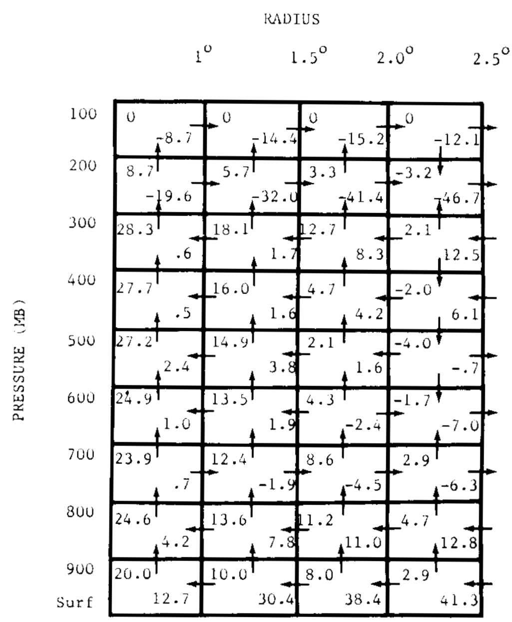

Fig. 17. Same as Fig. 15, except for 1800 GMT.

culation transports mass from the 100–200 mb layer down to the 200 to 300 mb layer where it is transported out of the 2.75° ring. Flow towards the cluster is also seen in the 300 to 400 mb layer.

In the growth-mature stage (1230 GMT composite) when deep convection is widespread, strong upward mass transport is confined to the cluster (Fig. 18). The cluster is enclosed with the 1.25°

ring. Most of the mass transported to the upper troposphere is supplied by the large scale flow of moist equatorial air from outside of the 2.25° ring, below 900 mb. Approximately 70% of the mass transported below 900 mb is removed in the 350 to 200 mb layer. The cluster is obviously responsible for the upward transport of moist low level air to the upper troposphere. A look at the upper level flow both relative to the cluster and the earth indicates that this transported mass is removed to higher latitides. This supports Riehl and Malkus's (1958) view that cloud clusters are the mechanisms responsible for the Hadley circulation cell.

Four scales of transport are examined. Large-scale convergence of the trades and monsoons provide for warm moist equatorial air to be transported upward through large cumulonimbi located inside the cloud cluster. The mass transported upward is then removed in the 300–200 mb layer, where the synoptic scale diffluence line lies. This mass is then transported northward to higher latititudes by planetary-scale circulations. Another interaction is implied if one considers the role of the easterly wave in providing for synoptic conditions favorable for cluster development (Reed and Recker, 1971; Burpee, 1972, 1974).

In the mature-dissipating stage (Fig. 17) 82% of the upward mass transport is still confined to the cluster. Lower level mass inflow from outside the 2.25° ring decreases by 23%. At the same time outflow increases by 23%. Weak outward horizontal mass flux from 600 to 400 mb is replaced by a net inward flux. This inward flux could be the cause of the cluster's dissipation allowing for the entrainment of dry middle tropospheric air, and the formation of mesoscale downdrafts: the resulting evaporative cooling of the lower levels would also aid in the dissipation of the cluster.

5. Summary and conclusion

The cluster under study is seen to develop in an area characterized by low-level confluence of the trades and monsoons, upper-level diffluence and mid-tropospheric easterly wave trough and undergo several stages of development. These stages can be seen by changes in the dynamic structure and by changes in the cloud morphology as seen in the satellite images. The resulting convergence is indicated in the satellite images as a long cloud line extending NW–SE.

An easterly wave approaching from the east sets up a dynamic condition favorable for the development of the cloud cluster. Strong easterly flow at 600 mb causes strong divergence in the middle troposphere during the growth stage of the cluster. Large values of cyclonic vorticity are present in the middle troposphere from a trough 100 km east of the cluster. The resulting instability favors the growth of cumulonimbus clouds along the cloud line. As cumulonimbi increase in height and area, the diffluence line at 250–200 mb provides for an efficient outflow mechanism.

Deep convective clouds are responsible in the growth-mature stage of the cluster for the observed dynamic mesoscale changes. The middle tropospheric divergence maximum becomes almost non-divergent. At the same time the 250 mb divergence maximum increases as upper levels become strongly divergent. Satellite images show this rapid increase in upper level divergence as an explosion of cirrus blow off. Strong low-level convergent inflow below 900 mb is roughly balanced by strong upper-level outflow from 250 to 200 mb. In this the most active stage of cluster development, the use of just satellite-derived lower and upper level winds can accurately describe the mass flux for this cluster. The increased upper tropospheric negative vorticity is the atmosphere's response to the increased divergence. Downward vertical motion above 600 mb in the growth stage becomes strongly upward in the growth to mature stage. Satellite images show a corresponding increase in the number and intensity of the cumulonimbi in the cluster. It was not possible to determine whether this increased vertical motion was the cause or effect of the observed increase in convection.

In the mature-dissipating stage the 250–200 mb divergence maximum becomes the dominant feature. In the satellite images this stage is indicated by the dominance of cirrus covering 110×10^3 sq. km. Low-level convergence decreases and becomes slightly divergent at 800 mb. From 700 to 325 mb weak convergence replaces the slightly divergent layer. Maximum vertical motion shifts from 800 to 300 mb. These changes are indicative of the dominance of deep clouds.

Mass flux computations show that the cluster forms in a broad area of large-scale convergence.

Mass is then transported upward to the middle troposphere. In the growth-mature stage, strong upward mass transport is concentrated in the region of the cluster. Air flows into the cluster from beyond 2.5° below 800 mb and is transported almost entirely out of the budget box area.

Four scales of transport are seen. Synoptic scale flow of the trades and monsoons converge along the ITCZ and transports mass upward through large cumulonimbi located inside the cloud cluster. The mass is then removed in the 300–200 mb layer, where the synoptic-scale diffluence line lies. Relative winds show this mass is then transported northward where planetary circulations can carry it to higher latitudes. Another interaction is implied as the easterly wave produces synoptic conditions favorable for the development of the cloud cluster.

This paper demonstrates that the kinematics and mass flux of an individual cluster can be successfully studied using a combination of satellite and conventional data in a composite format. Previously a study of this depth could only be done by compositing many clusters. It is important to note the similarities of this study to that done by Frank (1978) who composited many clusters over their various stages of development. Satellite studies done by Suchman et al. (1977) provide excellent horizontal data density at the inflow and outflow levels. However, at present individual cluster studies must utilize both satellite and conventional winds to study the cluster and its environment since satellites can not provide wind data in the middle troposphere with sufficient vertical resolution at present.

7. Acknowledgements

The authors with to thank Dr David W. Martin of Space Science & Engineering Center, University of Wisconsin at Madison for many valuable suggestions and comments during the preparation of this manuscript. The help of Brian Auvine in processing the data and the staff members associated with the McIDAS system at UW-Madison is greatly appreciated.

This research was supported by the National Science Foundation under Grant ATM76-16892.

REFERENCES

Burpee, R. W. 1972. The origin and structure of easterly waves in the lower trophosphere of North Africa. *J. Atmos. Sci. 29*, 77–90.

Burpee, R. W. 1974. Characteristics of North African easterly waves during the summers of 1968 and 1969. *J. Atmos. Sci. 31*, 1556–1570.

Frank, W. M. 1978. The life cycle of GATE convective systems. *J. Atmos. Sci. 35*, 1256–1264.

Houze, R. A. 1977. Structure and dynamics of a tropical squall-line system. *Mon. Wea. Rev. 105*, 1540–1567.

Leary, C. A. and Thompson, R. 1976. A warm-core disturbance in the western Atlantic during BOMEX. *Mon. Wea. Rev.* 443–452.

Leary, C. C. and Houze, R. A. 1979. The structure and evolution of convection in a tropical cloud cluster. *J. Atmos. Sci. 36*, 437–457.

Leary, C. A. 1979. Behavior of the wind field in the vicinity of a cloud cluster in the intertropical convergence zone. *J. Atmos. Sci. 36*, 631–639.

Mancuso, R. L. and Endlich, R. M. 1973. User's manual wind editing and analysis program: Spherical grid. WEAP-IA, Stanford Research Institute, Menlo Park, Calif., 69 pp.

Martin, D. W. and Suomi, V. E. 1972. A satellite study of cloud clusters over the tropical North Atlantic Ocean. *Bull. Amer. Meteor. Soc. 53*, 135–156.

Mosher, F. R. 1976. Cloud height determination. Proc. Symp. Meteorological Observations from Space: Their contributions to the First GARP Global Experiment, Philadelphia, Committee on Space Research, ICSU, 201–204.

Nitta, T. 1977. Response of cumulus updraft and downdraft to GATE A/B scale motion studies. *J. Atmos. Sci. 34*, 1163–1186.

O'Brien, J. J. 1970. Alternate solutions to the classical vertical velocity problem. *J. Appl. Meteor. 9*, 197–203.

Reed, R. J. and Recker, E. E. 1971. Structure and properties of synoptic scale wave disturbances in the equatorial western Pacific. *J. Atmos. Sci. 28*, 1117–1133.

Reed, R. J., Norquist, D. C. and Recker, E. E. 1977. The structure and properties of African wave disturbances as observed during phase III of GATE. *Mon. Wea. Rev. 105*, 317–333.

Reeves, R. W. 1978. GATE Convection Subprogram Data Center: Final report on rawinsonde data validation. *NOAA Tech. Rep. EDS 29*, 31 pp. (NTIS PB281861/5GA).

Riehl, H. and Malkus, J. S. 1958. On the heat balance in the equatorial trough zone. *Geophysica 6*, 503–538.

Riehl, H. 1954. Tropical Meteorology. McGraw-Hill.

Sikdar, D. N. and Suomi, V. E. 1971. Time variation of tropical energetics as viewed from geostationary altitude. *J. Atmos. Sci. 28*, 170–180.

Sikdar, D. N. and Suomi, V. E. 1972. On the remote sensing of mesoscale tropical convection intensity from a geostationary satellite. *J. Appl. Meteor. 11*, 37–43.

Smith, E. A. 1975. The McIDAS system. *IEEE Trans. Geosci. Electron. GE-13*, 123–136.

Smith, C. L., Zipser, E. J., Daggupaty, S. M. and Sapp, L. 1975. An experiment in tropical mesoscale analysis: Part I. *Mon. Wea. Rev. 103*, 878–892.

Suchman, D. and Martin, D. W. 1976. Wind sets from SMS images: An assessment of quality for GATE. *J. Appl. Meteor. 15*, 1265–1278.

Suchman, D., Martin, D. W. and Sikdar, D. N. 1977. Deep convective mass transport: An estimate from a geostationary satellite. *Mon. Wea. Rev. 105*, 943–955.

U.S. GATE Office 1977. Report of the U.S. GATE Central Program Workshop. National Center for Atmospheric Research, Boulder, CO., U.S.A. 723 pp.

КИНЕМАТИЧЕСКАЯ СТРУКТУРА ОБЛАЧНОГО СКОПЛЕНИЯ НАД АТЛАНТИКОЙ В ПЕРИОД АТЭП И ЕГО ИЗМЕНЕНИЕ СО ВРЕМЕНЕМ

В работе используется сеть тропосферного радиозондирования АТЭП (Атлантического тропического эксперимента ПИГАП) в тропиках вместе с данными с высоким разрешением о ветре с SMS-I (Синхронный метеорологический спутник) для определения временного хода кинематики и потока массы в область интенсивного облачного скопления, наблюдавшегося 5 сентября 1974 г. Спутниковые данные были приняты, продемонстрированы и обработаны на Системе выбора данных при взаимодействии человека и компьютера (McIDAS). Измерения расширения области с облаками в течение 20 часов определили стадии облачного скопления. Количественные измерения потока массы и кинематические свойства скопления даются для стадий роста, роста-зрелости и зрелости-рассеяния скопления. В фазе роста существует сильная конвергенция ниже 900 мб. Поле относительных ветров показывает, что приток массы к скоплению идет с запада-юго-запада ниже 950 мб в подоблачном слое. Сильная конвергенция низких уровней уменьшается по мере того, как на 250 мб становится доминирующей дивергенция. В стадии роста выше 600 мб существует движение вниз, которое становится направленным резко вверх по мере вызревания скопления. Максимальное вертикальное движение сдвигается с 800 к 300 мб в стадии зрелости-рассеяния.

Бюджет массы количественно описывает горизонтальный и вертикальный обмены массами внутри и вокруг скопления. В стадии роста воздух подоблачного слоя переносится горизонтально с расстояний, больших 300 км от центра скопления, переносится вверх в самом скоплении и находится в слое 800–600 мб. Стадия роста-зрелости, характеризуемая широко развитой глубокой конвекцией, показывает, что воздушная масса поднимается до уровня 200–250 мб, откуда она переносится к северу. Большая часть этой массы поставляется крупномасштабным потоком теплого влажного воздуха ниже 950 мб. Поле относительных ветров показывает, что глубокая конвекция в скоплении ответственна за перенос экваториального воздуха в верхних слоях к более высоким широтам, что поддерживает точку зрения о том, что облачные скопления являются интегральной частью циркуляции в ячейке Хэдли.